Analyst

Multicolour chemical imaging of plant tissues with hyperspectral stimulated Raman scattering microscopy

Journal:	*Analyst*
Manuscript ID	AN-ART-11-2020-002181.R1
Article Type:	Paper
Date Submitted by the Author:	07-Dec-2020
Complete List of Authors:	Iino, Takanori; The University of Tokyo, Department of Electrical Engineering and Information Systems Hashimoto, Kenji; Tokyo University of Science - Noda Campus, Department of Applied Biological Science Asai, Takuya; the University of Tokyo, Department of Electrical Engineering and Information Systems Kuchitsu, Kazuyuki; Tokyo University of Science Faculty of Science and Technology Graduate School of Science and Technology Applied Biological Science Ozeki, Yasuyuki; The University of Tokyo, Department of Electrical Engineering and Information Systems

ARTICLE

Multicolour chemical imaging of plant tissues with hyperspectral stimulated Raman scattering microscopy

Received 00th January 20xx,
Accepted 00th January 20xx

DOI: 10.1039/x0xx00000x

Takanori Iino,[*a] Kenji Hashimoto,[*b,c] Takuya Asai,[a] Kazuyuki Kuchitsu, [†b,c] and Yasuyuki Ozeki [†a]

Recent development of stimulated Raman scattering (SRS) microscopy allows for label-free biological imaging with chemical specificity based on molecular-vibrational signatures. In particular, hyperspectral SRS imaging can acquire molecular-vibrational spectrum at each pixel, allowing us not only to investigate the spectral difference of various biological molecules but also to discriminate different constituents based on their spectral difference. However, the number of constituents discriminated in previous label-free SRS imaging was limited to four because of the subtleness of spectral difference. Here, we report hyperspectral SRS imaging of plant tissues including leaves of *Camellia japonica*, roots of *Arabidopsis thaliana*, and thalli of a liverwort *Marchantia polymorpha L*. We show that SRS can discriminate as many as six components in *Marchantia polymorpha L.* without labeling. Our results demonstrate the effectiveness of hyperspectral SRS imaging as a tool of label-free multicolour imaging analysis of various biomolecules in plant tissues.

Introduction

Observing the distribution of various biomolecules is important for understanding the mechanism of living systems. Stimulated Raman scattering (SRS) microscopy[1-3] allows us to acquire molecular-vibrational images in real time, and has opened up a wide range of biological applications such as label-free imaging of biomolecules in various cells[4-7] and tissues[8-15], metabolic imaging,[16-19] and super-multiplex imaging.[20–21] Recently, several methods of hyperspectral SRS imaging are available,[22–26] which can acquire molecular-vibrational spectrum at each pixel to discriminate different chemical constituents, enabling multicolour label-free imaging. However, the capability of hyperspectral SRS microscopy to discriminate different molecules has not been fully exploited yet. Considering the ratio of the spectral width of typical biomolecules (~10 cm^{-1}) and the width of the carbon-hydrogen (C-H) stretching region (~200 cm^{-1}), hyperspectral SRS can, in principle, discriminate as many as >10 constituents based on the difference in their molecular-vibrational spectra. In reality, the number of constituents that can be discriminated by hyperspectral SRS imaging in the C-H stretching region is typically three or four because typical biological molecules tend to have similar spectra in the C-H stretching region.[5,22,26] Spectral phasor analysis of hyperspectral SRS images can classify five components in mammalian cells by utilizing the difference not only in spectral features but also in intensity,[27] but such classification discards morphological details. We should note that Raman imaging of plant tissues in the fingerprint region, where spectroscopic signatures are richer than C-H stretching region, followed by multivariate unmixing into six components has been reported.[28] However, Raman imaging suffers from various background signals, which can affect unmixing results, and therefore it still seems difficult to obtain consistent results among different unmixing algorithms.[28]

In this letter, we employ hyperspectral SRS microscopy in the C-H stretching region to demonstrate label-free multicolour imaging of intact plant tissues. Specifically, we present three-colour imaging of the leaves of *Camellia japonica*, four-colour imaging of the leaves as well as the tip and the middle part of the primary roots of *Arabidopsis thaliana*, and six-colour imaging of the thalli of a liverwort *Marchantia polymorpha L.* We anticipate that hyperspectral SRS microscopy is an effective tool of label-free imaging analysis of complex compositions of biomolecules in planta tissues.

Methods

Sample preparation

The biological samples were prepared as follows. A leaf of *Camelia japonica* was collected in the Noda campus of Tokyo University of Science, and its sections were cut at submillimeter thickness with a razor blade. Seedlings of *Arabidopsis thaliana* Col-0 were grown at 22 °C on 1% agar medium under continuous irradiation of white light for a week (in the case of the tip of the primary root) and for 5 weeks (in the case of the leaves and the middle of the primary root). Each tissue was clipped by using a surgical knife and

[a.] *Department of Electrical Engineering and Information Systems, The University of Tokyo, Tokyo 113-8656, Japan.*
[b.] *Department of Applied Biological Science, Tokyo University of Science, Noda 278-8510, Japan.*
[c.] *Imaging Frontier Center, Tokyo University of Science, Noda 278-8510, Japan.*
* These authors contributed equally.
† Corresponding authors: kuchitsu@rs.tus.ac.jp, ozeki@ee.t.u-tokyo.ac.jp
Electronic Supplementary Information (ESI) available: [details of any supplementary information available should be included here]. See DOI: 10.1039/x0xx00000x

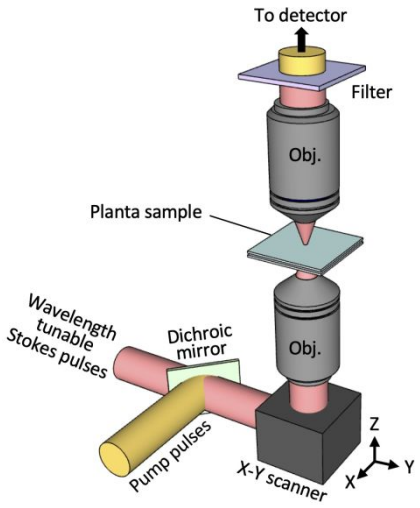

Fig. 1 A schematic of our home-made SRS microscope, which uses of (i) two-colour synchronized picosecond pump pulses and wavelength-tunable Stokes pulses, (ii) an X-Y scanner composed of a resonant galvanometric scanner and an ordinary galvanometric scanner to scan the laser beam, (iii) objective lenses to focus the pump and Stokes pulses onto the sample (the lower one) and to collect them transmitted through the sample (the upper one), and (iv) an optical filter that extracts pump pulses, which are detected by a Si detector connected to a home-made lock-in amplifier for acquiring the SRS signal.

tweezers. Young gemmalings of a liverwort *Marchantia polymorpha L.* were grown at 22 °C on 0.2% agar medium for a day. Each specimen was immersed in water, sandwiched by two cover slips, and then mounted on the stage of our SRS microscope.

SRS microscopy

The basic principle of SRS microscopy is as follows.[1-3] SRS microscopy employs two-colour trains of picosecond optical pulses at frequencies of $\boldsymbol{\omega_P}$ and $\boldsymbol{\omega_S}$, which are called as pump pulses and Stokes pulses, respectively. After high-frequency intensity modulation (>10 MHz) is applied to the Stokes pulse train, the pump and Stokes pulses are combined in time and space, and then focused on a sample. When the optical frequency difference between pump and Stokes (i.e., $\boldsymbol{\omega_P - \omega_S}$) matches the resonance frequency $\boldsymbol{\omega_R}$ of Raman-active molecular vibration in the focal volume, SRS is induced, which causes the attenuation of the pump pulses and the amplification of the Stokes pulses. As a result, the intensity modulation is transferred to the pump pulses. The transferred intensity modulation of pump pulses is detected to obtain the SRS signal. Images are taken by scanning the focal spot with a laser scanner.

Fig. 1 schematically shows our home-made SRS microscope, whose details are described elsewhere.[29] Briefly, we employ a Ti:sapphire laser (4 ps, 790 nm, 76 MHz, Mira 900-D, Coherent) as a pump pulse source and a wavelength-tunable Yb fibre laser system (5 ps, 1014–1046 nm, 38 MHz) as a Stokes pulse source, which is synchronized to the pump pulse source by a feed-back loop. The pump and Stokes beams are scanned with a X-Y scanner (8 kHz in the X direction and 30 Hz in the Y direction) and focused onto a sample with a water-immersion objective lens (60×, N.A. = 1.2, Olympus). The pump and Stokes pulse trains transmitted from the samples are collected using another water-immersion objective lens (60×, N.A. = 1.2, Olympus). After removing the Stokes pulse train using a short-pass filter with a cutoff wavelength of 930 nm, the pump pulses are detected by a Si photodiode. The output signal of the photodiode is delivered to the home-made lock-in amplifier to obtain SRS signal.

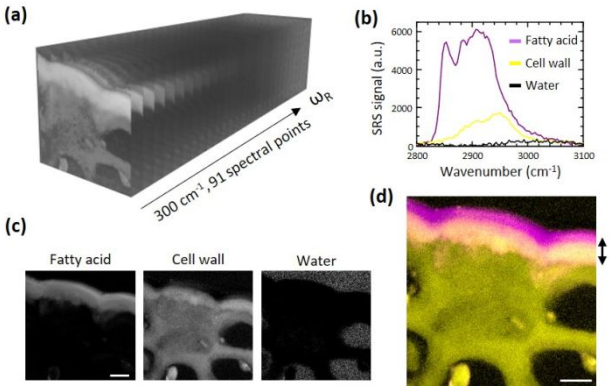

Fig. 2 SRS imaging of a leaf of *Camellia japonica*. (a) The schematic of the SRS image dataset of the cross-sectional area of the leaf, which is composed of 91 spectral images. Images were cropped for clarity. (b) Vibrational spectra used as the spectral bases. (c) The images of each constituent. (d) the multicolour image. The scale bars are 10 μm. The double-headed arrow indicates the cell wall-cuticle continuum.

As illustrated in Fig. 2(a), our SRS microscope can provide a hyperspectral image dataset, which can be decomposed to multicolour images in the following procedure. We assume that the measured hyperspectral SRS data $\boldsymbol{d_j}$ at the $\boldsymbol{j}$th pixel is a linear combination of the spectral bases $\boldsymbol{s_i}$ of the $\boldsymbol{i}$th constituent (e.g., fatty acid, lignin, and water, see Fig. 2(b)), namely, $\boldsymbol{d_j = \sum_i c_{ji} s_i}$. Here the coefficients $\boldsymbol{c_{ji}}$ are the concentrations of the corresponding constituents. Through pseudo matrix inversion[5] using the spectral bases that are manually picked up by investigating the morphology and spectral profiles, we obtain the concentration of each constituent at every pixel (Fig. 2(c)) as well as the multicolour images indicating spatial distributions of the constituents (Fig. 2(d)).

Throughout the experiments described below, each dataset is composed of SRS images acquired at 91 spectral points in the wavenumber region from 2800 to 3100 cm^{-1}, which covers the entire C-H stretching region. The image size is 500 pixels × 500 pixels and the field of view (FOV) is 80 μm × 80 μm. The image acquisition takes 3 s without averaging (*Camellia japonica*) and 30 s with the 10-times averaging (*Arabidopsis thaliana and Marchantia polymorpha L*). The optical power of pump and Stokes pulses at the sample plane was estimated to be ~50 mW and 70 mW, respectively.

Results

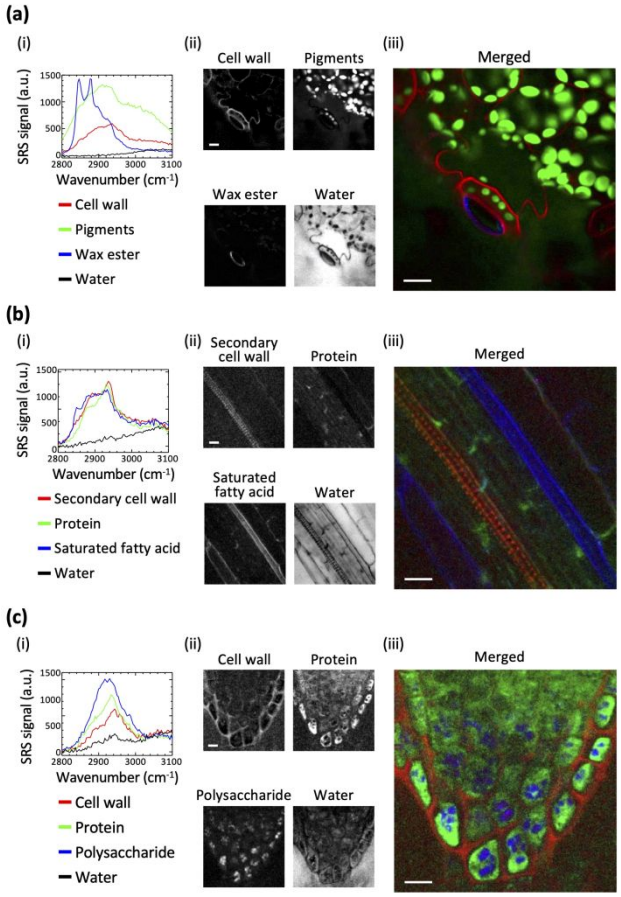

Fig. 3 SRS imaging of leaves and primary roots of *Arabidopsis thaliana*. (a) A rosette leaf. (b) The middle part of the primary root. (c) The tip of the primary root. (i), (ii), and (iii) show the extracted spectra used as the spectral base, the images of each constituent, and the merged SRS images, respectively. The merged images in (a)-(c)(iii) exhibit various structures such as (a) the cell wall (red), the chlorophyll (green), and the cuticle layer (blue), (b) the secondary cell wall (red), cytosol (green), and the suberin laminar on the lamellar existing on the surface of the endodermal cell (blue), and (c) the cell wall (red), cytosol (green), and amyloplast (blue). The scale bars are 10 µm.

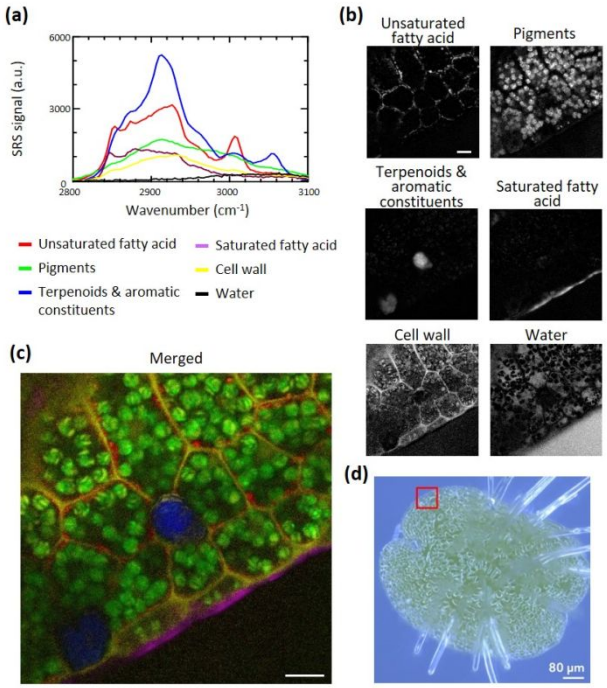

Fig. 4 SRS imaging of thalli of a liverwort *Marchantia polymorpha L.* (a) Extracted spectra used as the spectral bases. (b) Images of each constituent. (c) Merged SRS images exhibiting the following structures: lipid droplets (red), chlorophyll (green), oil body (blue), the cuticle layer (magenta), the cell wall (yellow). The scale bars: 10 µm. (d) A photograph of an entire gemmaling of *Marchantia polymorpha L*.

First, we demonstrate the SRS imaging of a section of a leaf of *Camellia japonica*. Fig. 2(a) illustratively shows the dataset of the leaf. From the measured hyperspectral SRS data, the spectral bases were manually extracted (Fig. 2(b)). From spectral shapes and morphology, the extracted spectra are speculated to be those of cell wall (yellow line),[12,30] which exhibits a peak at 2940 cm^{-1} (CH_3 stretching mode), saturated fatty acids (magenta line),[12,31] which exhibit a flat response from 2850 to 2930 cm^{-1} (alkyl chain), and water (black line)[32,33] that originates from the low-wavenumber tail of the OH-stretching mode at ~3200 cm^{-1}. The images of the respective constituents are shown in Fig. 2(c). The resultant multicolour image is shown in Fig. 2(d), where the morphologies of magenta- and yellow-coloured sites are consistent with those of the cuticle wax layer and cell wall.[34] Remarkably, the overlapped distribution of these constituents (yellowish brown-coloured site indicated by double-sided arrow) confirmed the cell wall-cuticle continuum,[35] which works in regulating the molecular transportation into and out of plant body, affecting the response to diverse pathogen infections.[36]

Fig. 3 shows the SRS images of *Arabidopsis thaliana* that is a typical model species in plant molecular biological and genetic research. Specifically, we conducted hyperspectral SRS imaging of rosette leaves and the middle part and the tip of primary roots. In all *Arabidopsis* samples, we were able to decompose the SRS datasets into four constituents. Specifically, in rosette leaves (Fig. 3(a)), the extracted spectra are speculated to be those of cell wall (the red line), pigments (the green line),[5] which exhibit broad spectral response due to two-photon absorption, wax esters (the blue line),[12] which exhibits sharp peaks at 2850 and 2880 cm^{-1}, and water (the black line). The spatial distributions of the decomposed components were consistent with the cellular morphology; cell wall, chloroplasts, and cuticle wax layer, respectively.

In the middle part of primary roots (Fig. 3(b)), four spectra were discriminated and speculated to be those of secondary cell wall (the red line), protein (the green line)[22,25] which exhibits a peak at 2930 cm^{-1} with a smaller signal at 2910 cm^{-1} than lignin, saturated fatty acids (the blue line), which exhibit a flat response from 2850 to 2930 cm^{-1} (alkyl chain), and water (the black line). Again, the spatial

distributions of the decomposed components were consistent with the morphology of the secondary cell wall in the conduit,[37,38] cytosol, and the suberin lamellar, which seems to exist on the surface of the endodermal cells, implying that Casparian strip, a band of cell wall materials such as suberin deposited in the radial and transverse walls of the endodermis, was visualized.[39–41]

In the tip of the primary root (Fig. 3(c)), the spectra were speculated to be cell wall (red line), protein (green line), polysaccharide (blue line),[42,43] which has a peak at 2910 cm^{-1}, and water (black line). The spatial distributions of the decomposed components are consistent with the morphologies of the cell wall, cytosol, and amyloplasts which accumulate starch.[44] In this way, using the SRS microscopy, we can acquire four-colour images in a label-free manner.

Fig. 4 shows the SRS images of a thallus of *Marchantia polymorpha L.*, where six spectra were extracted (Fig. 4(a)) and used as spectral bases. The extracted spectra are speculated to be those of unsaturated fatty acids (red line) which exhibit a broad spectrum ranging from 2850 to 2930 cm^{-1} (alkyl chain) with a sharp peak at 3010 cm^{-1} (C-H stretching mode associated with a carbon-carbon double bond), pigments (green line), secondary metabolites contained in the oil bodies that may be a highly diverse mixture of terpenoids and aromatic constituents (blue line),[45] which exhibit strong peaks at 2910 cm^{-1} (CH_2 antisymmetric stretching mode) and 3050 cm^{-1} (aromatic C-H stretching mode), saturated fatty acid (magenta line), cell wall (yellow line), and water (black line). Fig. 4(b) shows the spatial distribution of the decomposed components, which are consistent with the morphology of the lipid droplets, chloroplasts, oil bodies, cuticle wax layer, and cell wall.[45] Fig. 4(c) shows the merged SRS image of thallus (Fig. 4(d)), demonstrating the label-free six-colour imaging by hyperspectral SRS imaging.

Discussion

We demonstrated the multicolour label-free imaging of various types of plant tissues by utilizing hyperspectral SRS imaging, which allows us to discriminate tiny spectral difference through the linear unmixing method.[5] Hyperspectral SRS imaging will particularly be useful for the imaging analysis of complex structures of plant tissues, in which autofluorescence from pigments accumulated in intracellular organelles such as chloroplasts, cell wall and the vacuole often prevent fluorescence imaging. Furthermore, once we obtain a hyperspectral SRS dataset, we can look into it to find various biomolecules to produce multicolour images. This is in contrast to previous reports on SRS imaging of plant tissues with a few spectral points,[11-15] where specific biomolecules in plant tissues such as wax ester and lignin were investigated.

An important technical challenge is the automatic classification of constituents in the hyperspectral SRS dataset. In this work, spectral bases were manually extracted by investigating SRS spectra at many pixels, which is labour-intensive, heuristic, and time-consuming. As mentioned before, spectral bases are manually picked up from a dataset. If they do not reflect pure components, the images given by pseudo-matrix inversion reflect mixtures of components. Furthermore, if some spectral bases are not linearly independent, pseudo-matrix inversion gives noisy images, and this suggests the number of components. At the moment, we haven't succeeded in quantifying the accuracy of the spectral analysis. Although various algorithms of automatically extracting spectral bases[22,26,46,47] or of classifying different cellular components[27] have been proposed, it still seems difficult to extract as many as six components using these algorithms.[28] It will be of importance to develop a classification method based on the morphological and hyperspectral features to fully utilize the capability of hyperspectral SRS imaging.

Conclusions

To summarize, we have demonstrated the hyperspectral SRS microscopy of plant tissues for label-free multicolour imaging of up to six components utilizing the molecular discrimination capability of hyperspectral SRS microscopy. We anticipate that, with the development of better spectral extraction methods, we should be able to fully utilize the power of the hyperspectral SRS microscopy as a label-free multicolour imaging analysis tool of plant tissues.

Conflicts of interest

There are no conflicts to declare.

Acknowledgements

This work is partially supported by JST CREST (Grant Number JPMJCR1872), Japan, and Quantum Leap Flagship Program of MEXT (Grant Number JPMXS0118067246), Japan, and Imaging Frontier Center, Tokyo University of Science.

References

1 C. W. Freudiger, W. Min, B. G. Saar, S. Lu, G. R. Holtom, C. He, J. C. Tsai, J. X. Kang and X. S. Xie, *Science,* 2008, **322**, 1857.
2 P. Nandakumar, A. Kovalev and A. Volkmer, *New J. Phys.,* 2009, **11**, 033026.
3 Y. Ozeki, F. Dake, S. Kajiyama, K. Fukui and K. Itoh, *Opt. Express,* 2009, **17**, 3651.
4 F.-K. Lu, S. Basu, V. Igras, M. P. Hoang, M. Ji, D. Fu, G. R. Holtom, V. A. Neel, C. W. Freudiger, D. E. Fisher, and X. S. Xie, Proc. Natl. Acad. Sci. U. S. A., 2015, **112**, 11624.
5 Y. Wakisaka, Y. Suzuki, O. Iwata, A. Nakashima, T. Ito, M. Hirose, R. Domon, M. Sugawara, N. Tsumura, H. Watarai, T. Shimobaba, K. Suzuki, K. Goda and Y. Ozeki, *Nat. Microbiol.*, 2016, **1**, 16124.
6 Y. Suzuki, K. Kobayashi, Y. Wakisaka, D. Deng, S. Tanaka, C.-J. Huang, C. Lei, C.-W. Sun, H. Liu, Y. Fujiwaki, S. Lee, A. Isozaki, Y. Kasai, T. Hayakawa, S. Sakuma, F. Arai, K. Koizumi, H. Tezuka, M. Inaba, K. Hiraki, T. Ito, M. Hase, S. Matsusaka, K. Shiba, K. Suga, M. Nishikawa, M. Jona, Y. Yatomi, Y. Yalikun, Y. Tanaka, T. Sugimura, N. Nitta, K. Goda and Y. Ozeki, *Proc. Natl. Acad. Sci. U. S. A.,* 2019, **116**, 15842.
7 T. Asai, H. Liu, Y. Ozeki, S. Sato, T. Hayashi and H. Nakamura, *Appl. Phys. Express,* 2019, **12**, 112004.
8 B. G. Saar, C. W. Freudiger, J. Reichman, C. M. Stanley, G. R. Holtom and X. S. Xie, *Science,* 2010, **330**, 1368.

9 M. Wei, L. Shi, Y. Shen, Z. Zhao, A. Guzman, L. J. Kaufman, L. Wei and W. Min, *Proc. Natl. Acad. Sci. U. S. A.,* 2019, **116**, 6608.
10 M. Egawa, S. Iwanaga, J. Hosoi, M. Goto, H. Yamanishi, M. Miyai, C. Katagiri, K. Tokunaga, T. Asai and Y. Ozeki, *Sci. Rep.,* 2019, **9**, 12601.
11 J. C. Mansfield, G. R. Littlejohn, M. P. Seymour, R. J. Lind, S. Perfect, and J. Moger, *Anal. Chem.,* 2013, **85**, 5055.
12 G. R. Littlejohn, J. C. Mansfield, D. Parker, R. Lind, S. Perfect, M. Seymour, N. Smirnoff, J. Love and J. Moger, *Plant Physiol.,* 2015, **68**, 18.
13 B. Liu, P. Wang, J. I. Kim, D. Zhang, Y. Xia, C. Chapple, and J. -X. Cheng, *Anal. Chem.,* 2015, **87**, 9436.
14 Y. Zeng, J. M. Yarbrough, A. Mittal, M. P. Tucker, T. B. Vinzant, S. R. Decker and M. E. Himmel, *Biotechnol. Biofuels,* 2016, **9**, 216.
15 N. Zhu, Y. Yang, M. Ji, D. Wu and K. Chen, *Horticulture Research,* 2019, **6**, 72.
16 J. Li, and J. X. Cheng, *Sci. Rep.,* 2014, **4**, 6807.
17 L. Zhang, L. Shi, Y. Shen, Y. Miao, M. Wei, N. Qian, Y. Liu, and W. Min, *Nat. Biomed. Eng.,* 2019, **3**, 402.
18 L. Wei, F. Hu, Y. Shen, Z. Chen, Y. Yu, C. C. Lin, M. C. Wang, and W. Min, *Nat. Methods,* 2014, **11**, 410.
19 K. Midorikawa, K. Tsuchiya, S. S. Y. Law, Y. Miyagi, T. Asai, T. Iino, Y. Ozeki, Y. Kodama, and K. Numata, RSC Chem. Biol. (advance publication).
20 L. Wei, Z. Chen, L. Shi, R. Long, A. V. Anzalone, L. Zhang, F. Hu, R. Yuste, V. W. Cornish, and W. Min, *Nature,* 2017, **544**, 465.
21 F. Hu, C. Zeng, R. Long, Y. Miao, L. Wei, Q. Xu and W. Min, *Nat. Methods,* 2018, **15**, 194.
22 Y. Ozeki, W. Umemura, Y. Otsuka, S. Satoh, H. Hashimoto, K. Sumimura, N. Nishizawa, K. Fukui and K. Itoh, *Nat. Photonics,* 2012, **6**, 845.
23 Y. Ozeki, W. Umemura, K. Sumimura, N. Nishizawa, K. Fukui and K. Itoh, *Opt. Lett.,* 2012, **37**, 431.
24 L. Kong, M. Ji, G. R. Holtom, D. Fu, C. W. Freudiger and X. S. Xie, *Opt. Lett.,* 2013, **38**, 145.
25 D. Fu, G. Holtom, C. Freudiger, X. Zhang and X. S. Xie, *J. Phys. Chem. B,* 2013, **117**, 4634.
26 D. Zhang, P. Wang, M. N. Slipchenko, D. Ben-Amotz, A. M. Weiner and J.-X. Cheng, *Anal. Chem.,* 2013, **85**, 98.
27 D. Fu and X. S. Xie, *Anal. Chem.,* 2014, **86**, 4115.
28 B. Prats-Mateu, M. Felhofer, A. de Juan and N. Gierlinger, *Plant Methods*, 2018, **14**, 52.
29 Y. Ozeki, T. Asai, J. Shou and H. Yoshimi, *IEEE J. Sel. Top. Quantum Electron.,* 2019, **25**, 7100211.
30 N. Gierlinger and M. Schwanninger, *J. Spectrosc.,* 2007, **21**, 69.
31 K. Czamara, K. Majzner, M. Z. Pacia, K. Kochan, A. Kaczor and M. Baranska, *J. Raman Spectrosc.,* 2015, **46**, 4.
32 G. E. Walrafen, *J. Chem. Phys.,* 1964, **40**, 3249.
33 B. M. Auer and J. L. Skinner, J. Chem. Phys., 2008, **128**, 224511.
34 P. Erxu, P. Qiufa, L. Hongfei, S. Jingbo, D. Yueqiang, H. Feilai and H. Hui, *Bot. J. Linn. Soc.,* 2009, **159**, 456.
35 C. Nawrath, L. Schreiber, R. B. Franke, N. Geldner, J. J. Reina-Pinto, and L. Kunstc, *Arabidopsis Book*, 2013, **11**, e0167.
36 C. Ziv, Z. Zhao, Y. G. Gao, and Y. Xia, *Front. Plant Sci.,* 2018, **9**, 1088.
37 Y. Oda and H. Fukuda, *Curr. Opin. Plant Biol.,* 2012, **15**, 38.
38 N. Vukašinović, Y. Oda, P. Pejchar, L. Synek, T. Pečenková, A. Rawat, J. Sekereš, M. Potocký and V. Žárský, *New Phytol.,* 2017, **213**, 1052.
39 J. Graça, *Front. Chem.,* 2015, **3**, 62.
40 N. Geldner, *Curr. Biol.,* 2013, **23**, R1025.
41 S. Naseer, Y. Lee, C. Lapierre, R. Franke, C. Nawrath and N. Geldner, *Proc. Natl. Acad. Sci. U. S. A.,* 2012, **109**, 10101.
42 M. R. Almeida, R. S. Alves, L. B. L. R. Nascimbem, R. Stephani, R. J. Poppi and L. F. C. de Oliveira, *Anal. Bioanal. Chem.,* 2010, **397**, 2693.
43 R. Kizil and J. Irudayaraj, *J. Agric. Food Chem.,* 2006, **54**, 13.
44 E. B. Blancaflor, *Am. J. Botany,* 2013, **100**, 143.
45 M. Shimamura, *Plant and Cell Physiol.,* 2016, **57**, 230.
46 J. M. P. Nascimento and J. M. B. Dias, *IEEE Trans. Geosci. Remote Sens.,* 2005, **43**, 898.
47 A. Alfonso-García, J. Paugh, M. Farid, S. Garg, J. Jester and E. Potma, *J. Raman Spectrosc.,* 2017, **48**, 803.